Public summary of the list of material properties and selection guide for Los Humeros North

Deliverable 8.5

Public summary of the list of material properties and selection guide for Los Humeros North

Deliverable 8.5

Responsible author: Ingólfur Þorbjörnsson (ÍSOR)

Responsible SP leader: Jan Diederik van Wees (TNO)

Responsible WP leader: Ernst Huenges (GFZ)

Contributions by: Luis Eduardo Gonzales (Geominco), Miquel Ramirez (CFE), Lilibeth Morales (CFE), Heber Diez (CFE), Sigurður S. Jónsson (ISOR), Gunnar S. Kaldal (ISOR), Lárus Guðmundsson (ISOR)

PU - Public

Work package 8.2

The GEMex project is supported by the European Union's Horizon 2020 programme for Research and Innovation under grant agreement No 727550

Table of Contents [1]

List of figures

[1] The content of this report reflects only the authors' view. The Innovation and Networks Executive Agency (INEA) is not responsible for any use that may be made of the information it contains.

List of tables

Executive summary

This report is a public open summaty of the D 8.2 – List of materials peroperties and selection guide for Los Humeros North.

Selection of materials for high-temperature geothermal wells follows oil and gas (O&G) standards and recommendations and the same applies for wellhead design, well design and drilling. Geothermal wells differ from O&G wells with higher temperatures, in chemistry of steam/brine and higher amount of non-condensable gases such as H_2S and CO_2 and often low pH level. These are all parameters that have corrosive effect on the well material and often more complicated forms of corrosion are observed in geothermal use than in common O&G wells. It is therefore of high importance for long life of geothermal wells to select casing materials that can both withstand the high temperature and the corrosive nature of the geothermal fluid. The goal of the work documented here, is to test the corrosive nature of geothermal environment against candidate materials for use in Los Humeros geothermal field in Mexico and to compare that with previous tests in Icelandic geothermal fields. For comparison with older results a selection of "stand alone" materials were tested but some are also prime candidate materials for cladding. Testing was done as downhole testing were the testing material was attached to a hexagonal bar acting as a sample holder and lowered down to 1290 m depth in superheated well H-64 in Los Humeros. Duration of test was two weeks in the well.

1 Introduction

This report is a public open version of the deliverable 8.2 within the GEMex project – a cooperation between European and Mexican partners.

Deliverable 8.2 have primary focus on Task 8.2 – Materials for installation in super-hot systems and contribute to Task 8.3 drilling and completion.

For material suitable for use in the geothermal industry, scientists and material providers have actively been looking into the corrosion nature of geothermal steam and brine for many years. This has resulted in better material selection for geothermal use, mainly in the surface equipment like valves, steam separators, pipes and not least in the turbines. More recently the focus has been moving over to the wells, traditionally designed according to O&G standards with respect to materials. In this deliverable the focus will be on testing materials downhole where geothermal steam is in direct contact with the samples with downhole conditions. The corrosive nature of the geothermal steam/brine is highly site dependent; the corrosive aggressiveness of geothermal fluids can vary from sour wells in volcanic sites to dry wells in older geothermal systems. The effect of non-condensable gases is of high importance, especially the partial pressure of H_2S that can trigger material cracking as Hydrogen Induced Cracking (HIC) or as SSCC (Sulphide Stress Corrosion Cracking). Beside the effect of low pH and amount of gases one must look to free halogens such as Chloride (Cl^-) which can trigger pitting corrosion and general corrosion. Material selection for a given well is clearly not a straight forward task, as it must be based on the site-specific conditions. Today the selection is based on API (American Petroleum Institute) and NACE (National Association of Corrosion Engineers) standard and guidelines of materials, selected and designed for Oil and Gas wells. The materials that are most common are low/medium carbon grades and in most cases these material grades have proven to be successful. Today many wells with these materials have been in operation for over 30 years. Going into deeper and higher temperature fields generate furthermore increased interest in the materials as the more aggressive fluid in deeper geothermal sites calls for more resistant material solutions.

2 Corrosion in geothermal wells

Corrosion in geothermal wells has been in research focus for many years. The importance of understanding why corrosion occurs and the chemical reaction of the material surface with geothermal fluid is of high importance for long life of geothermal wells. The pH level together with geothermal gases and free halogens like Cl^- are known corrosion factors (Thorbjornsson, 1995).

Materials in dry superheated steam wells have shown to be affected by Hydrogen Embrittlement but generally the materials (API grades: K55, L80, T80, T95) used for the well casing and liner have shown to be long lasting. Exceptions are buckling and formation of so-called bulges in the production casing resulting from stresses in the material because of thermal expansion during warming up of the well.

2.1 Material testing in geothermal environment

Materials used in high temperature/pressure geothermal fluid can be subjected to corrosion due to the aggressiveness of the geothermal fluid and non-condensable gases such as hydrogen sulphide (H_2S) and carbon dioxide (CO_2), chloride ions (Cl-) and hydrogen fluoride (HF) as described earlier. The fluid composition varies from one field to another and even between wells in the same area. Further the geothermal fields have the tendency to change in the gas content during utilization and build-up of scaling can be important for the resistance of materials to corrosion.

2.2 Uniform corrosion

Uniform corrosion is the most common corrosion form for carbon and low alloy steels. This form of corrosion requires moisture or other electric conducting media on the surface were anode-cathode reaction can take place. This corrosion is measured on coupons where they are weighted before and after testing. The weight loss is related to the surface area of the coupons and often represented as corrosion rate in mm/year. General acceptance for corrosion rate in geothermal environment is not set by standards but often the acceptance limit is set to 0.1 mm/year. This form of corrosion is more often discovered on the outside of wells, especially at the wellhead were the casings exceed from the cement. This is mostly due to the fact that it is not possible to measure or detect degradation due to corrosion in well material down-hole.

General corrosion is characterised by the following anode-cathode reaction:

- Anode: $M \rightarrow M^{n+} + ne^-$
- Cathode: $O_2 + 2H_2O + 4e^- \rightarrow 4OH^-$ or

  $2H^+ + 2e^- \rightarrow H_2$

The oxygen reaction is the dominant cathodic reaction if pH > 5.5 and there is oxygen present. Hydrogen evolution increases rapidly at pH $\leq$ 5.5 and gradually becomes the dominant reaction.

The absence of a fast-cathodic reaction often limits corrosion in geothermal systems.

The anodic reaction produces metal ions M^{n+}. The metal ions generally combine with other ions in the electrolyte to form a solid corrosion product on the metal surface were the most common of these is rust which consists of iron oxides and hydroxides, $Fe(OH)_3$ - Fe_2O_3 (hematite, red rust) or Fe_3O_4 (magnetite, black rust). In highly acid fluids, little or no solid corrosion products are generally formed on the corroding metal surface.

2.3 Pitting corrosion

Pitting corrosion is highly localized corrosion forming cavities or holes in the metal surface. The starting points for pit formation in steel are often MnS inclusions or other impurities in the metal surface. For steels containing passive films such as stainless steels the local destruction of the passive film is commonly due to presence of chlorides. The resistance of pitting for steels can be calculated according to the Pitting Resistance Equivalent Number (PREN) and can be used for comparison between different types of steels, mostly stainless steels. The PREN is calculated according to standard ISO 15156-3 Materials for use in H_2S containing environments and the formula is given as:

$$PREN = \%Cr + 3.3\ (\%Mo + \%W) + 16\ \%N$$

For common stainless steels used in the geothermal industry the PREN value is:

- ASTM 304 PRE ≈ 19
- ASTM 316 PRE ≈ 25
- ASTM S31803 PRE ≈ 35
- ASTM S32750 PRE ≈ 43
- ASTM NO904L PRE ≈ 35
- ASTM 31254 PRE ≈ 43
- ASTM 32654 PRE ≈ 56

2.4 Hydrogen damage

Geothermal gases contain Hydrogen Sulphide, H_2S, but the amount varies from field to field. H_2S is a known hydrogen recombination poison (catalytic poison) that increases the ratio of absorbed hydrogen to cathodically produced hydrogen. As a result, the introduction of atomic hydrogen into a metal by corrosion in wet H_2S may be significant. Atomic hydrogen will diffuse into the metal and may pass through the metal or stop (be trapped) at sites that interact more strongly with hydrogen than the lattice sites, e.g., grain boundaries, carbides, micro voids, slag inclusions or other defects. Hydrogen damage is the collective term for several failure mechanisms that may occur when hydrogen is introduced to the metals. Some damage mechanisms relevant for geothermal conditions are described below.

Hydrogen attack is the term used when atomic hydrogen in the metal reacts with carbon to produce methane gas which causes cracks and fissures in the metal. Hydrogen attack may occur in carbon steels at temperatures from 200 to 600 °C.

Hydrogen induced cracking (HIC) describes the formation of blisters and cracks due to the pressure from atomic hydrogen recombining to gaseous H_2 at defects inside the metal. HIC may occur at temperatures up to 150 °C without applied or residual stress. A phenomenon that may be experienced for stainless steel clad or weld overlaid steels is hydrogen induced disbonding (HID), where blisters form at the bond/fusion line between the steel and the stainless alloy. The large difference in hydrogen solubility between an austenitic clad metal and a ferritic substrate may give large hydrogen concentrations at the interface when cooling after operation at elevated temperature.

Hydrogen embrittlement (HE) describes the embrittlement or cracking resulting from the combination of tensile stress and atomic hydrogen in the metal. Sulphide stress cracking (SSC) is the cracking due to atomic hydrogen introduced in a H_2S environment and as such a special case of HE. HE of ferrous alloys is most severe around room temperature. The trapping of hydrogen at defects diminishes at increasing temperature, while at lower temperatures diffusion of atomic hydrogen in the metal is slowed down. The risk for HE/SSC in a geothermal well is therefore largest when the temperature drops, e.g., during a production stop. The experience from operating wells in these fields have not showed any incidents like cracking of the well casing materials.

2.5 Stress corrosion cracking

Stress corrosion cracking (SCC) is phenomena were stress, material composition and environmental effects play a vital role. SCC is often connected to, but not only, use of stainless steels of the austenitic type. When tested in geothermal the use of prestressed specimen is used. Various kinds of damages, crack-like, can be found in metal alloys subjected to SCC.

2.6 Galvanic corrosion

Galvanic corrosion is due to metallic connection between two metals of different chemical composition with electrolyte on the surface. Metals have different steady-state electrode potential according to their composition.

Connecting two alloys in electrolyte, such as water, can lead to anode-cathode reaction where the less noble metal will dissolve to give electrons to protect the nobler alloy.

In a geothermal well with cladded pipes as casing, galvanic corrosion problems should not occur, since the clad material would be the only one in contact with the geothermal fluid as innermost casing. Galvanic corrosion refers to corrosion damage when two dissimilar metals are coupled in a corrosive electrolyte. The driving force will be the electric potential difference between the dissimilar materials. For cladded pipes the carbon steel alloy base, which has the most positive electrode potential compared to the clad materials, and thereby is the less noble one due to relative nobility in the galvanic series, would become the anode and corrode faster than it would all by itself, while the clad material corrodes slower than it would alone.

On a microstructural level, micro galvanic couples could be formed between phases or other microstructural features could be subject to galvanic currents.

3 Materials for geothermal wells

Materials for geothermal wells have mainly been from low and medium carbon steels were the wells casings and liners are from API types, such as J55, K55, L80 and T95 steels. In recent years and specially to cope with very sour wells the use of Titanium casings (Salton Sea USA) and cladding like in IDDP-1 were the expansion spool was weld cladded with 309 type stainless steels. In the following sections each material type will be discussed.

3.1 Carbon steels

Carbon steels or low alloy steels with less than 0.25% C and 0.4-1.5% Mn are the dominating materials used for geothermal wells, for pipes and equipment above ground. In general, this material has shown to be both economic and long lasting for geothermal wells. Materials mainly used in Icelandic high temperature wells are API K55 grade. API TN95 has been used were higher strength and creep resistance is required like in the uppermost section of the IDDP-1 well. In general, carbon steels have shown long lasting properties in geothermal use, with the exception were the pH level has dropped and when condition has allowed condensation on the material surface. Above ground in diverse equipment the carbon steels have suffered from erosion-corrosion. However, carbon steels are good candidates for use in controlled conditions where condensate can be avoided and where erosion-corrosion is not a problem.

3.2 Stainless steels

Stainless steels are steels containing more than 12% Cr and are often alloyed further with Ni, Mo and N. Stainless steels have a wide use in applications in the geothermal power production, mainly in diverse equipment's and piping. They have not been used for casings in geothermal wells in Iceland. In general, this material group can be divided into two major groups when used in geothermal fields, Austenitic stainless steels and Duplex stainless steels. Both groups have long history of use in geothermal fields in Iceland and have been proven as a proper material for wide variety of applications. For higher temperatures above 250°C it is not recommended to use the Duplex type due to its structural change, shown as change in the material tensile strength and ductility above that

temperature. Below 250°C the Duplex types S32507 and S32707 have both excellent resistances to corrosion. The Austenitic types can in fact be divided into two types, the lower alloyed types AISI 304 and AISI 316 and then the higher alloyed 254 SMO (S31254), N08904 and N08028. The 304/316 types have shown to have limited resistance to corrosion in geothermal conditions and suffer from diverse corrosion forms in high temperature steam. The higher alloyed austenitic steels have shown better performance, especially the S31254 type. In general, the stainless steels, especially the higher austenitic grades, can be considered as good candidate materials for use in high temperature geothermal steam with temperatures above 250°C.

3.3 Nickel alloys

Nickel based alloys with Nickel content below 60% have long tradition for being good materials for diverse harsh environments such as geothermal environment. These alloys have not been widely used in geothermal steam in Iceland so limited practical experience has been obtained. Further testing of these materials is needed for better clarification of their use in high temperature geothermal steam.

3.4 Titanium

Two types of titanium alloys have previously been tested in the superheated well IDDP-1 in Iceland at 450°C, type R50400 and R52400. The R50400 type suffered from narrow pitting but the R52400 type alloyed with Pd showed more resistance. There is some concern with regard to HF containing steam like in IDDP-1 for the R50400 type were the R50400 has more resistance to HF containing steam due to the Pd alloying. In general, the concern of strength for Titanium alloys can limit their use at higher temperatures (>400°C). The possibility of hydrogen embrittlement is also of concern for low pH environment at higher temperatures (>80°C).

4 Testing of materials in Los Humeros

For testing materials for corrosion resistance in a geothermal well there are several options. First is the surface test that can be carried out in the steam pipe, either the main pipe to the power plant or the one leading to the silencer. Another option for surface testing is to pipe steam from the main steam pipe into test tank and even into an autoclave system. The types of surface testing previously used in Iceland are shown in Figure 1.

.

Figure 1. *Surface testing. On the left steam pipe to the silencer with sample rack as shown in the middle picture. On the right corrosion tank with steam inlet from the main steam pipe.*

Another option for testing is downhole testing. Downhole testing is primary selected to enable testing of casing candidate materials in real conditions downhole in the well, preferable in blending zone between fluid from two fractures or in conditions with liquid from one selected fracture. Downhole testing is though more demanding than surface testing as the testing material is lowered into the well by wire line and the risk of material loss is severe. Downhole testing also puts limitation on size and volume of the testing material. Samples need to be fully insulated from the sample holder and bolts, this is shown in Figure 2.

Figure 2. *Sample rack for downhole testing. Hexagonal bar with attached samples on the left ready for downhole testing in well in Iceland (Karlsdottir and Thorbjornsson 2013). On the right drawing showing how ceramic washers are used to ensure no metal to metal contact between sample and test bar.*

Consultation between partners about testing procedure resulted in decision that the testing would be carried out as downhole testing based on previous experience from Iceland (Karlsdottir and Thorbjornsson, 2013). For testing in Los Humeros, it was therefore decided that the testing time would be limited to two weeks to ensure that the wire used for lowering the test bar into the well would not be affected by the corrosive environment downhole and selection of materials would include non-cladded materials preferable the same as have been tested in Iceland for comparison.

4.1 Los Humeros – selection of well

For well to be tested, partner CFE selected well H-64 in north Los Humeros geothermal fields. Well H-64 was selected due to it's harsh conditions, low pH and superheated conditions.

4.1.1 Well design and conditions

The selected well H-64 was drilled and completed 2017. The well is 2310 m vertical, and as it is deviated its total length is 2360 m. In Figure 3 the completion of well H-64 is with 13⅜" anchor casing set at 500 m, kick-off at 1000 m and 9⅝" production casing to 1300 m. The well is then with perforated 7" liner down to its total depth of 2310 m. Materials for the casings are according to API 5 CT standard, K55 for anchor casing and T80-Cr3% for production casing and perforated liner.

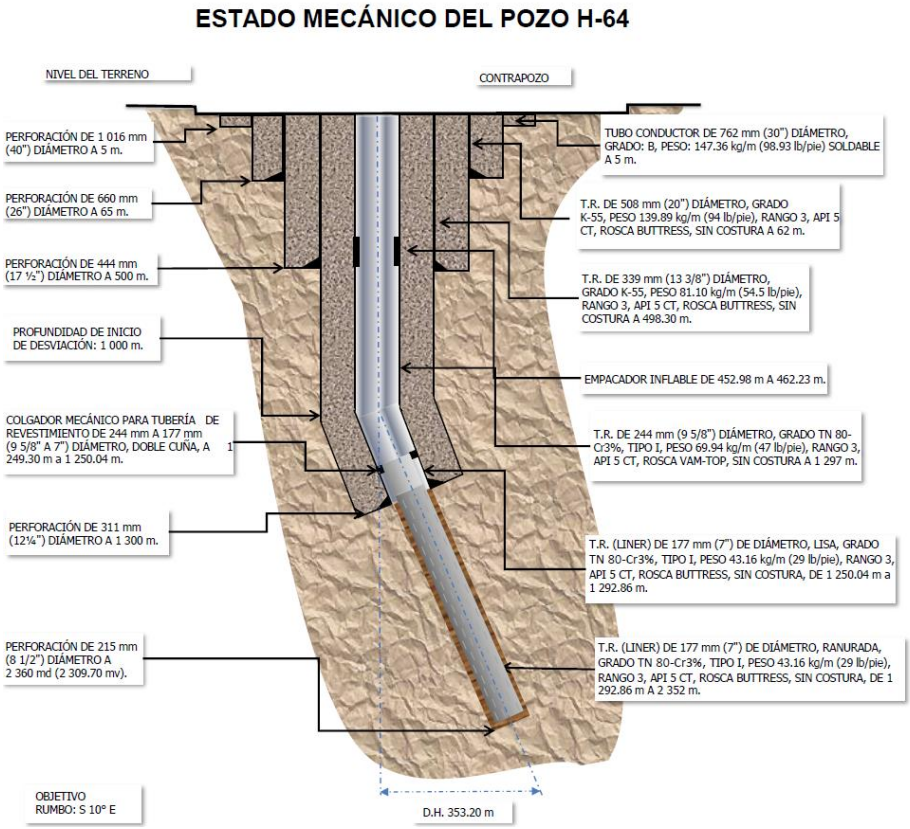

Figure 3. *Well H-64 as build. Drawing from CFE.*

Temperature and pressure was measured prior to testing. Profiles can be seen in Figure 4. As can be seen from the saturation profile the well has superheated conditions from 200 m depth. This means that the conditions are pure steam as can be seen on the pressure log which gives pressure around 38-40 bar at wellhead to around 45 bar at 2300 m. Before testing, production rate from the well was around 13 t/h with well head pressure 38 bar and temperature around 250°C with flow controlled by orifice plate with 31.75 mm hole (1.25”). After two weeks of testing the conditions had changed, production rate was measured around 11 t/h with well head pressure of 28 bar.

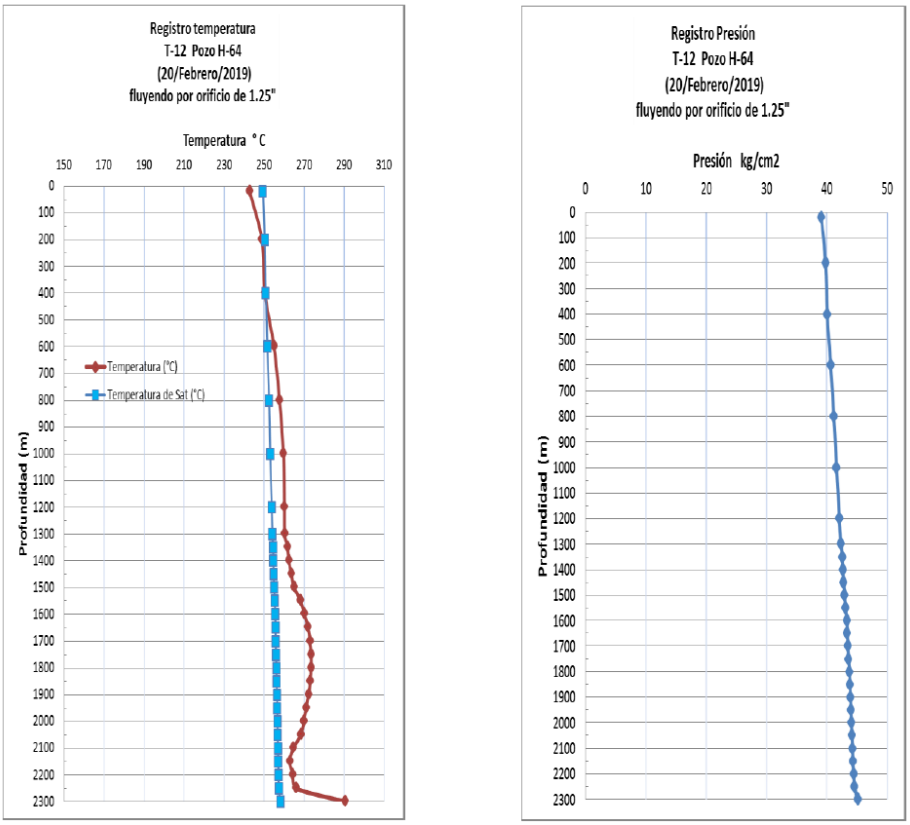

Figure 4. *Temperature profile with saturation and measured temperature on the left and pressure profile on the right. Source CFE.*

4.1.2 Chemical composition.

Chemical composition of steam from H-64 was measured three times, on the 20th and 21st of February and on the 7th of March 2019. The testing in H-64 started on the 21st of February and ended on the 7th of March.

Table 1. *Chemical composition of well H-64. For comparison the chemical composition from two wells in Iceland are given. Three values are given from H-64, measured on the 20th and 21st of February and from 7th of March 2019. Symbol ! is used to indicate no data available. Some values for H-64 were only measured on the 20th of February.*

	Los Humeros Superheated H-64 [ppm]	**Reykjanes Condensated steam RN-35 [ppm]**	**Krafla Superheated IDDP-1 [ppm]**
pH	3.77 – 5.4 – 3.7	4.06 / 22°C	2.44 /22.7°C
Conductivity µS/Cm	674 -360 - 1184	138 / 25°C	977 / 25°C
Cl	173.58 – 102.9 – 330.07	16.3	!
B	164.476 – !0 – 181.716	0.51	2.2
Na	0.1 – 1.31 – 0	5.51	0.08
Ca	1.172	!	<0.1
SiO_2	73 – ! – 20.37	!	6.2
HCO_3	3.6 - ! – 0	!	!
SO_4	9.1 - ! – 6.962	!	!
Mg	0.0865	!	0.004
Fe	43.04 – 19.56 – 66.67	!	21.5
TDS	1952.155 – 123.771 – 555.062	42	70

An important factor for the chemical analyses are the presence of F that was found in XRD analyses of scaling from the carbon steel K55. F was not measured during the chemical campaign but as found by Tello et al. (2000), the presence of HF is found in the steam phase at Los Humeros.

Gas content was measured twice in H-64, on the start of testing at the 21st of February and when the samples were retrieved from the well on the 7th of March 2019.

Table 2. *Measured gases in the steam at H-64 and comparison given to two Icelandic wells.*

	Los Humeros Superheated H-64 [ppm]	Reykjanes Condensated steam RN-35 [ppm]	Krafla Superheated IDDP-1 [ppm]
CO_2	27065 – 31407	5620	560
H_2S	4622 – 3930	235	250
H_2	33.82 – 30.33	0.67	8.77
N_2	388.21 – 351.29	71.4	16.3
CH_4	3.26 – 0.73	1.61	0.27
Ar	27.97-8.31	2.02	0.53
NH_3	11.04 – 68.59	!	!

5 Materials for testing

For testing in well H-64 in Los Humeros a selection of materials was done. Materials were selected from five material groups:

Medium carbon steel – Common used in Geothermal Industry for casings.

Austenitic stainless steels – Candidate material for cladding and as a stand-alone material.

Nickel alloy – Candidate material for cladding and as a stand-alone material.

Titanium – Candidate material for stand-alone material.

Duplex stainless steels – Candidate material for up to 250°C, cladded and as a stand-alone.

The selection of grades within each group are based on research already performed in Icelandic high temperature fields. (Thorbjornsson et al., 2015; Karlsdottir et al. 2015). In Table 3 the materials selected are shown.

Table 3. *Materials selected for testing in H-64 in Los Humeros Mexico.*

No.	Type	Name
SA01	Carbon steel	API K55
SA05	Austenitic SS	S31266 (B66)
SA06	Nickel alloy	N06022 (C-22HS)
SA08	Titanium	R56320 (Grade 9)
SA10	Nickel based alloy (SS)	NO6625 (UR625)
SA14	Super Duplex SS	S32507 (UR2507)
SA17	Austenitic SS	S31254 (254 SMO)

Table 4. *Chemical composition given by standard for the selected materials.*

	C %	Mn	Cr	Ni	Mo	N	Ti	Cu	Other
API-K55	-	-	-	-	-	-	-	-	P <0,03 S <0,03
S31266	<0,03	2-4	23-25	21-24	5,2-6,2	0,35-0,6		1-2,5	W 1,5-2,5
N06022	<0,10	<0,5	20-22,5	Balance	12,5-14,5	-	-	-	Co <2,5 W 2,5-3,5 V <0,35
R56320	<0,08	-	-	-	-	<0,03	Ballance	-	Al 3 V 2,5
N06625	0,03-0,10	<0,5	20-23	>58	8-10	-	< 0,4	<0,5	Nb 3,15-4,15 Co <1,0 Fe <5,0
S32507	<0,03	0,5-1,2	24,5-26,0	6-8	3-5	0,24-0,32	-	<0,5	Si 0,1-0,8
S31254	<0,02	<1,0	19,5-20	17,5-18	6-6,5	0,18-0,2	-	0,5-1	Si <0,8

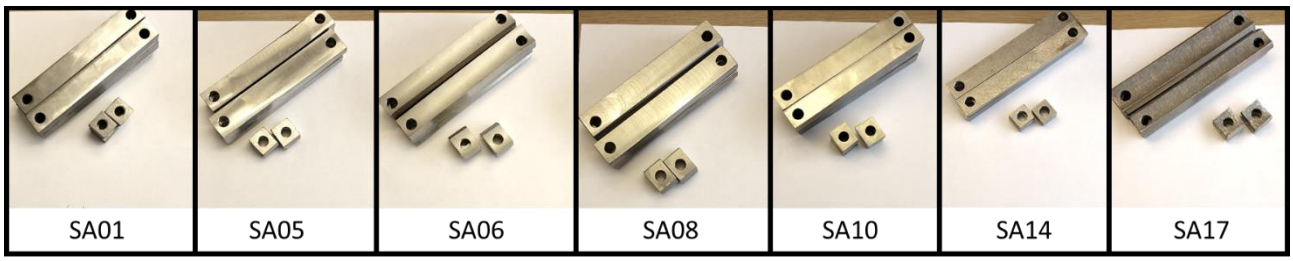

Figure 5. *Figure showing the samples used in Los Humeros. Three larger specimens and two smaller of each material was used for downhole testing.*

6 Testing in well H-64

Downhole testing in well H-64 started on the 21st of February. The hexagonal bar with 35 samples from 7 materials shown in Table 3, were lowered down to 1290 m depth. The original plan was to go deeper, to 1350 m but due to some obstacles in the well it was not possible to reach that depth. As can be seen in Figure 3 the production casing end in 1300 m and therefore the test bar was close to the end of the production casing, at the top of the perforated liner. The hexagonal test bar, 1.03 m in length and 79.4 mm in diameter with samples, was made from carbon steel. Slickline wire used was Hastelloy C-276 with 0.092" or 2.3 mm diameter. Before lowering the test bar with samples, all samples were measured to make sure that no electrical conductivity was between samples and the hexagonal bar. At the end of the hexagonal bar a balloon like centralizer was attached. The setup before testing is shown in Figure 6. In Figure 7 lubricator for lowering the samples downhole as well as the hexagonal bar with centralizer and samples can be seen.

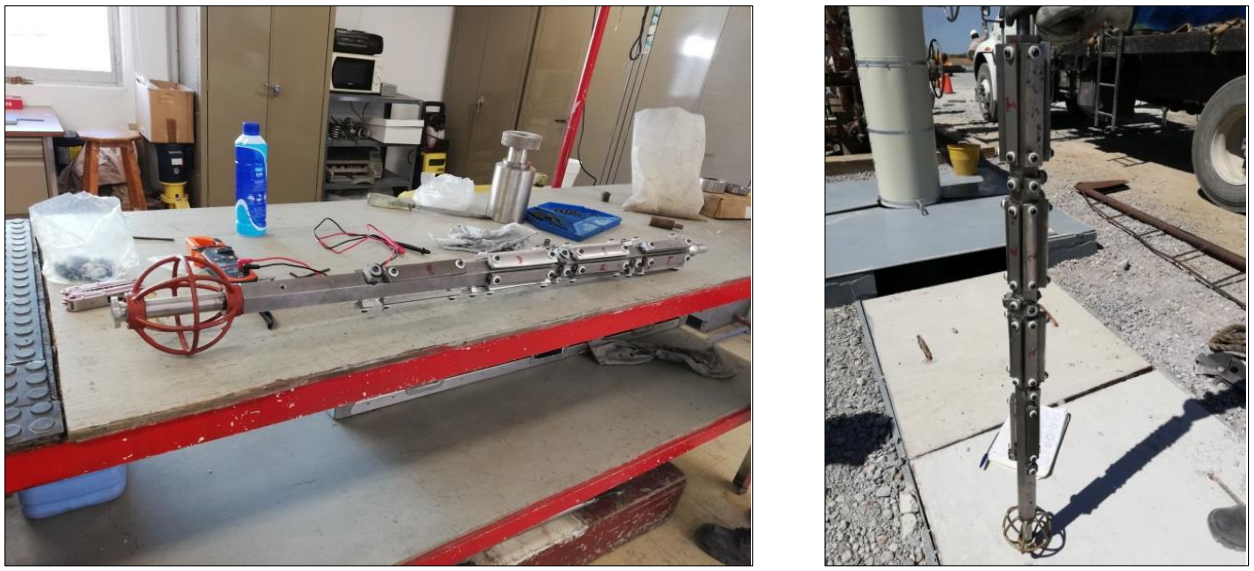

Figure 6. *Hexagonal test bar with test samples. Pictures from CFE.*

Figure 7. *Preparations at well head for lowering the hexagonal sample holder with samples downhole. Pictures from CFE.*

Testing started on the 21st of February 2019, time was14:34 were the bar was lowered into the well and at15:30 it had reached the testing depth of 1290 m. The test bar was then retrieved from the well with all specimens safely to the surface on the 7th of March at time 9:42. At surface the test bar was securely transported to CFE facilities and inspected visually. As shown in Figure 8 the hexagonal test bar, centralizer and samples are covered by grey coloured scaling after two weeks in the well.


Figure 8. *Pictures showing the hexagonal bar as retrieved.*

7 Corrosion

After testing for two weeks sample racks were removed from the well and samples removed from the hexagonal sample holder. All samples were packed in plastic separate. The samples were then transported to the project coordinator at UNAM University. At a meeting between ÍSOR and Geominco the samples were divided, one of the larger samples and all weight loss coupons were transported to ISOR and three of the larger samples were given to Geominco for slow strain testing and microstructural analyses (not reported in this deliverable).

7.1 XRD

Samples of materials, approximately 20 mm by 10 mm and 150 mm long, tested in a geothermal well in Mexico for a period of two weeks were analysed (Figure 9). Of all the samples used in the experiment, a few had notable surface deposits. The secondary deposits were removed from the samples using a stainless steel surgical scalpel and the material collected was ground and deposited onto a quarts (zero-background) sample holder using organic solvent (acetone). A Bruker AXS D8 Focus diffractometer was used (Bragg-Brentano goniometer), with Ni-filtered Cu kα radiation at 1.54 Å wavelength at 40 mA and 40 kV, with fixed 1° slits and NaI scintillation counter. Scanning range is from 2Θ=4-64°, with a step-size of 0.02°and measurement time of 1 second in each step. Interpretation of the results was done using a Diffrac.Suite EVA software from Bruker, associated with PDF-2 2019 database from ICDD.

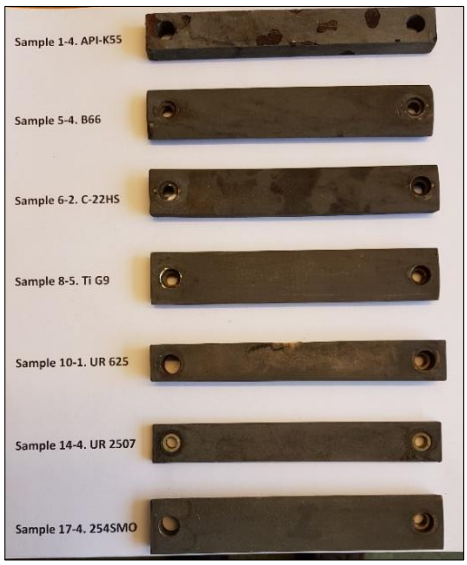

Figure 9. *Samples as received from testing. Samples for XRD analyses were taken from scaling on sample 1-4, 5-4, 14-4 and 17-4.*

Sample 1-4 (upper surface): Material API K55 was with visible severe scaling and corrosion as can be seen in Figure 9. Scaling revealed with microscopic inspection to be twofold, an upper layer and close to the steel a layer with notable difference from the upper layer. XRD analysis was conducted on both layers, here referred to as "upper surface" and "sub surface". As seen in Figure 10, the material is iron-rich, manifested by the high background radiation caused by fluorescence of iron (red pattern) in the radiation wavelength produced by the Cu-anode. On the lower pattern the background radiation has been subtracted. Of the readily identifiable phases, pyrrhotite is abundant and magnetite is also notable. Boron-containing compounds match with considerable confidence. Sodium fluoride is also noted but due to the simple symmetry of such materials it is difficult to confirm its presence. Two large peaks were not found to match with any suggested and likely candidates and thus remain unresolved (at 2Θ=34.8° and 49.1°).

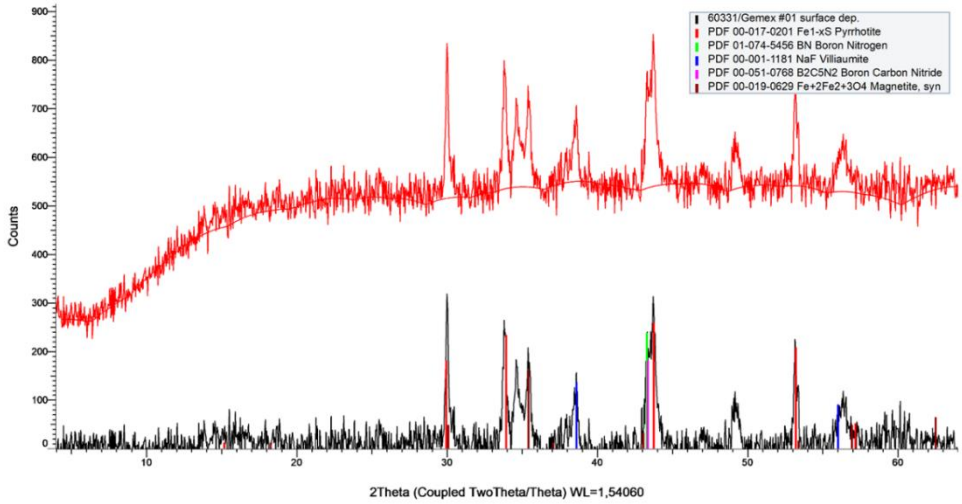

Figure 10. *X-ray diffraction pattern of corrosion scaling on sample 1-4 (API K55) upper layer. The sample's pattern is shown both raw (red) and with background subtraction (lower pattern). Legend shown refer to dif-patterns from ICDD PDF-2019.*

Sample 1-4 (sub-surface): The immediate surface below the surface deposit is mostly comprising pyrrhotite, but sodium fluoride and boron compounds could also be present (Figure 11).

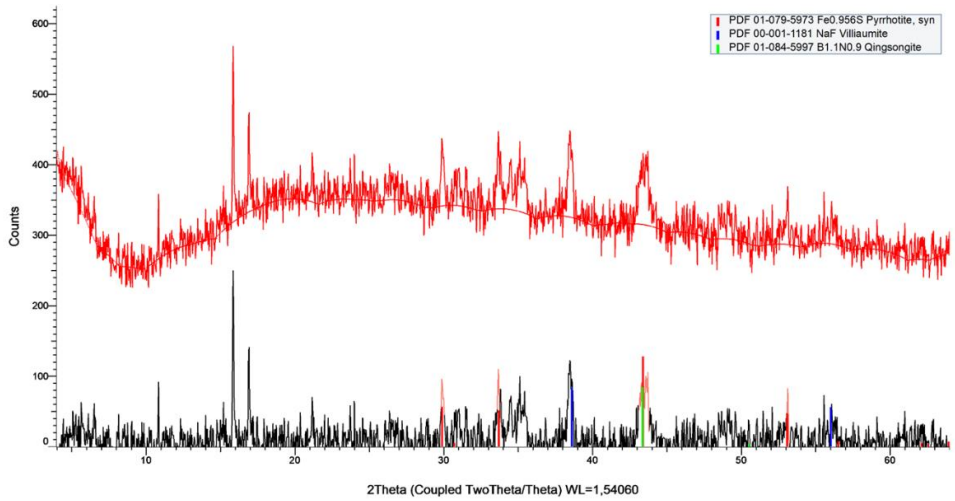

Figure 11. *X-ray diffraction pattern of corrosion scaling on sample 1-4 (API K55) sub layer. The sample's pattern is shown both raw (red) and with background subtraction (lower pattern).*

Sample 5-4 (surface deposit): This sample from the super austenitic steel S31266 (B66), is entirely comprising pyrrhotite and magnetite. High iron content is manifested by high and characteristic background radiation (Figure 12).

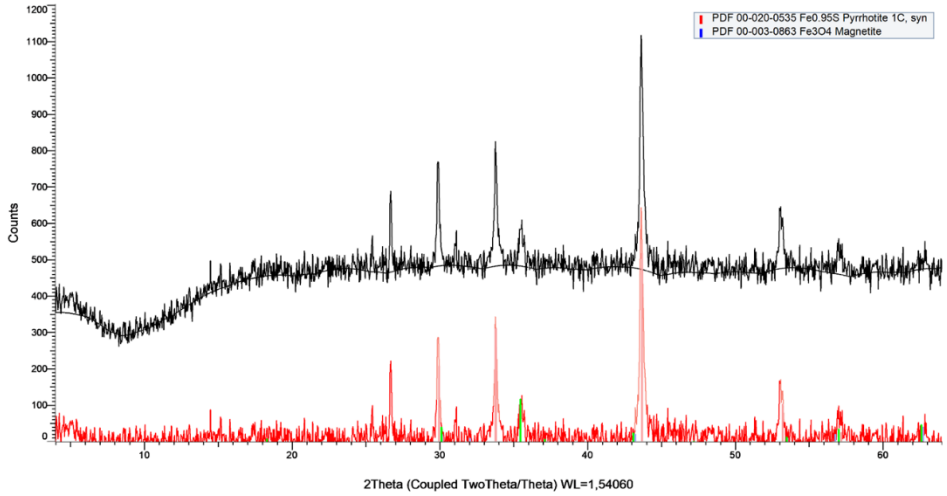

Figure 12. *X-ray diffraction pattern of corrosion scaling on sample 5-4 (Super austenitic stainless steel S31266; B66) up. The sample's pattern is shown both raw (black) and with background subtraction (lower pattern).*

Sample14-4 (surface deposit): This sample from the super Duplex steel S32507 reveal that magnetite is the only phase that seems to be present in the scale (Figure 13).

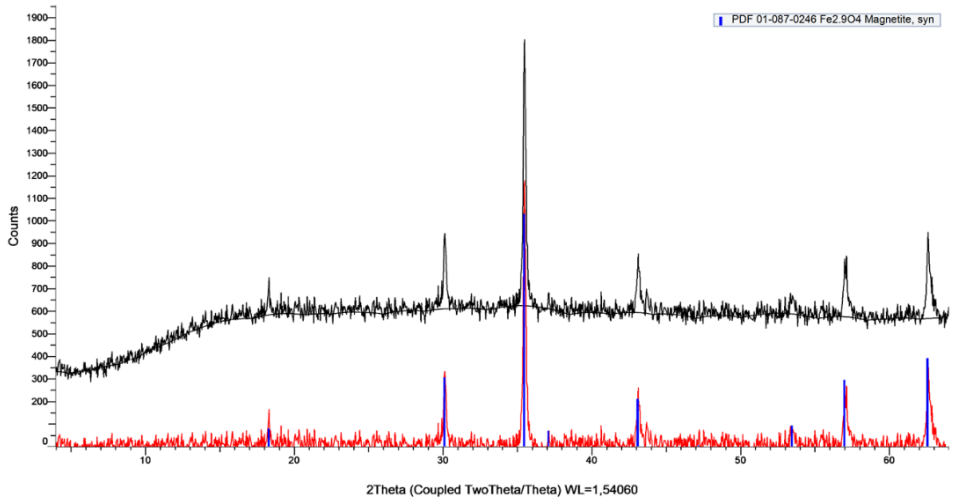

Figure 13. *X-ray diffraction pattern of corrosion scaling on sample 14-4 (Super Duplex 32507) upper layer. The sample's pattern is shown both raw (black) and with background subtraction (lower pattern).*

Sample 17-4 (surface deposit): This sample from the Super austenitic steel S31254 reveal that pyrrhotite is only present in the scale (Figure 14).

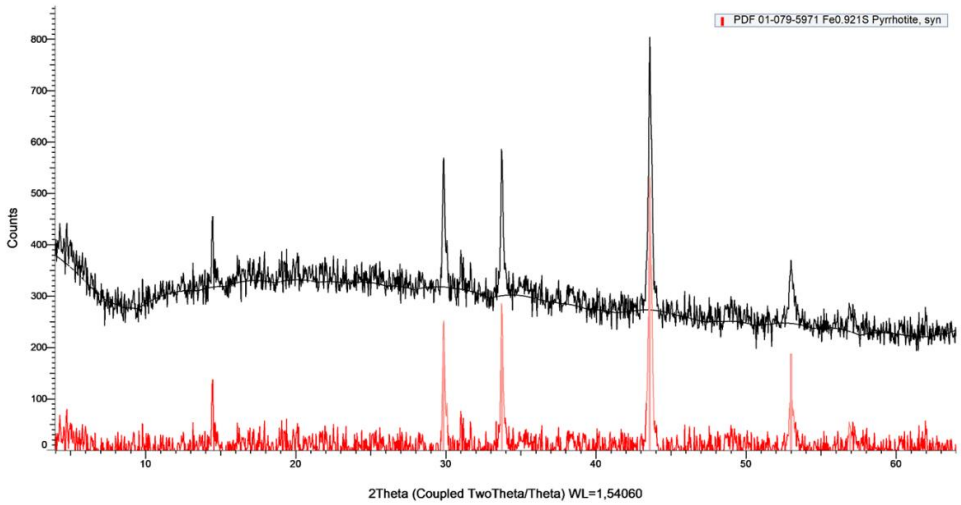

Figure 14. *X-ray diffraction pattern of corrosion scaling on sample 17-4 (Super Austenitic stainless steel S31254) upper layer. The sample's pattern is shown both raw (black) and with background subtraction (lower pattern).*

7.2 Weight loss measurement

Before shipping to Los Humeros for testing, all samples were weighted with precision scale OHAUS Explorer Pro EP214C see Figure 15. After testing the samples for weight loss measurements, were at arrival at ÍSOR stored in a desiccator. After each cleaning step the samples were weighted, and results compared with original weight before testing.

7.2.1 Cleaning

The following cleaning procedures used for cleaning samples, based on their alloying elements and in accordance with ASTM G1 (ASTM G1, 2017). Samples were cleaned before initiating the cleaning procedures dictated by the standard ASTM G1. The samples were placed in an ultrasonic cleaner with isopropanol for 10 minutes, repeated three times over.

All samples were weighed between each procedure.

Cleaning procedure for all samples before weight loss measurements:

- ✓ Samples weighted as received from autoclaves.
- ✓ Samples were lightly brushed and rinsed with deionized water.
- ✓ Samples placed in an ultrasonic bath with isopropanol for 10 minutes.
- ✓ Samples dried in an oven for 1 hour at 100°C.

- ✓ First cleaning process in accordance with ASTM G1:
    - C.3.5 Iron and steel cleaning solution for 10 minutes.
        - Samples SA-01
    - C.6.1 Nickel & nickel alloys cleaning solution for 1-3 minutes.
        - Samples: SA-06, SA-08, SA-10
    - C.7.1 Stainless steel cleaning solution for 20 minutes.
        - Samples: SA-05, SA-14, SA-17
    - Samples dried in oven for 1 hour at 100°C

- ✓ Samples were placed in an ultrasonic cleaning bath with isopropanol for 10 minutes and dried in an oven for 1 hour at 100°C.

- ✓ Second chemical cleaning process in accordance with ASTM G1. Chemical cleaning:
    - C.7.1 stainless steel cleaning solution for 20 minutes.
    - C.3.5 Iron & steel cleaning solution for 10 minutes.
    - C.6.1 nickel & nickel alloys cleaning solution for 1-3 minutes.
    - Samples dried in oven for 1 hour at 100°C

- ✓ Samples cleaned in an Ultrasonic cleaning bath with isopropanol for 10 minutes and then dried in an oven for 1 hour at 100°C.

Samples were weighed on an OHAUS Explorer Pro EP214C as shown in Figure 15.

Figure 15. *Precision scale, OHAUS Explorer Pro EP214C, used for weight loss measurement*.

Cleaning steps and weighting after each step were stopped after 10 steps.

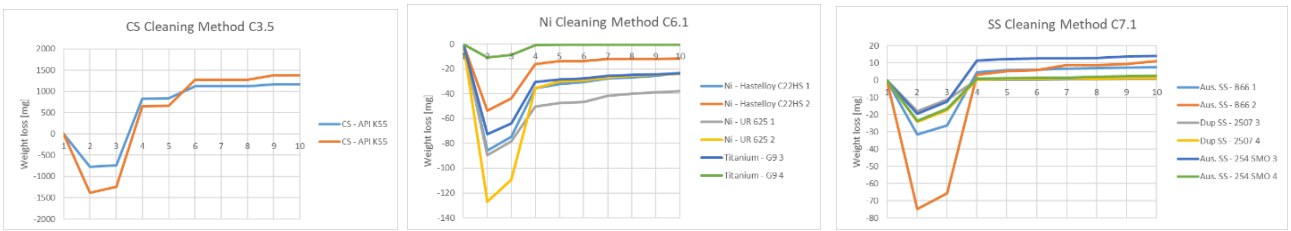

Figure 16. *Measured weight loss after each cleaning step. On the left weight loss for the carbon steel, in the middle nickel alloys and Titanium and on the right the super austenitic and duplex steels. Note that the scale is not the same between materials.*

7.2.2 Weight loss

Samples from downhole testing in Los Humeros were weighed before shipment to Mexico, after two weeks of testing the samples for weight loss were transported to Iceland and cleaned as discussed in 7.2.1. In Figure 17 the samples are shown as recieved from testing. Some scaling were observed on the samples and due to the scaling the first weighing shown in Figure 16, showed increase in weight compared to the weight as shipped to Mexico. For medium carbon steel grade K55 and stainless steel grades the scaling was removed with cleaning but for the Nickel and Titanium grade it was not possible to remove the scaling fully as shown in Figure 16.

.

Figure 17. *Samples for weight loss measurement before cleaning. Two samples were tested for each material.*

Table 5. *Measured corrosion rate for all weight loss coupons.*

Material	Coor. Rate [mm/year]
CS - API K55	2,051
CS - API K55	2,568
Aus. SS -S31266 (B66)	0,015
Aus. SS – S31266 (B66)	0,022
Ni – NO6022 (C22HS)	0,000
Ni – NO6022 (C22HS)	0,000
Titanium - R56320 (G9)	0,000
Titanium - R56320 (G9)	0,000
Ni – NO6625 (UR 625)	0,000
Ni – NO6625 (UR 625)	0,000
Dup SS – S32507 (2507)	0,002
Dup SS – S322507 (2507)	0,003
Aus. SS – S31254 (254 SMO)	0,027
Aus. SS – S31254 (254 SMO)	0,005

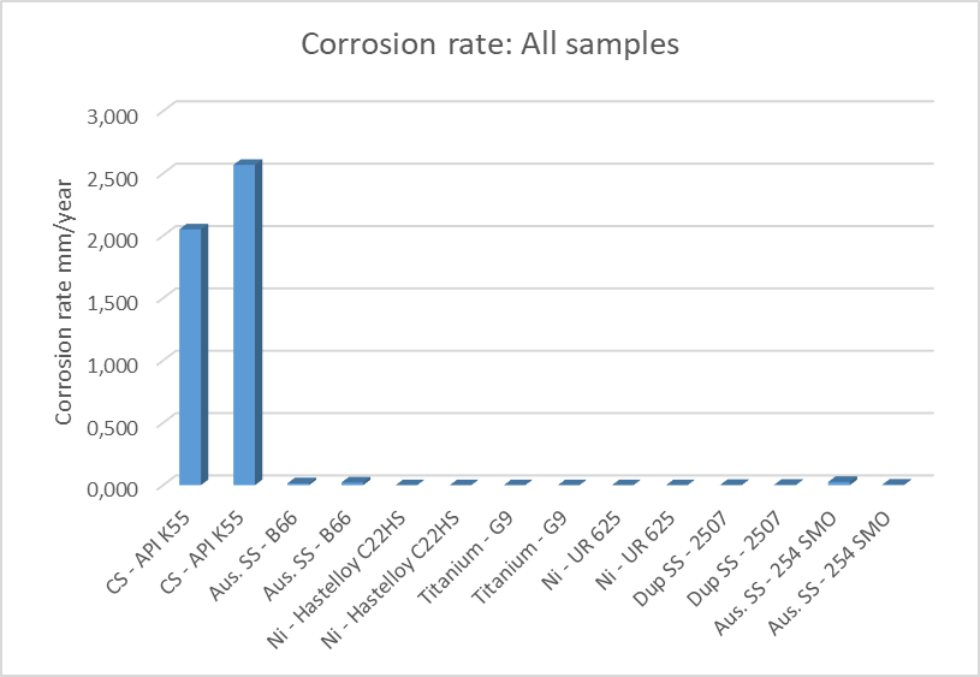

Figure 18. *Measured corrosion rate for all tested weight loss coupons.*

As shown in Figure 18 the corrosion rate for the carbon steel API-K55 is much higher than for the corrosion resistant alloys (CRA) tested. In Figure 19 the CRA corrosion rate are shown for both coupons tested for each CRA. As noted for S31254 (254 SMO) the values are not consistent, and the higher value are higher than expected. Also, it is to be noted that the higher alloyed S31266 (B66) (Table 4) gives higher corrosion rate than the lower alloyed S31254. This is consistent with testing in superheated steam in Iceland as shown in Figure 22 and Figure 23.

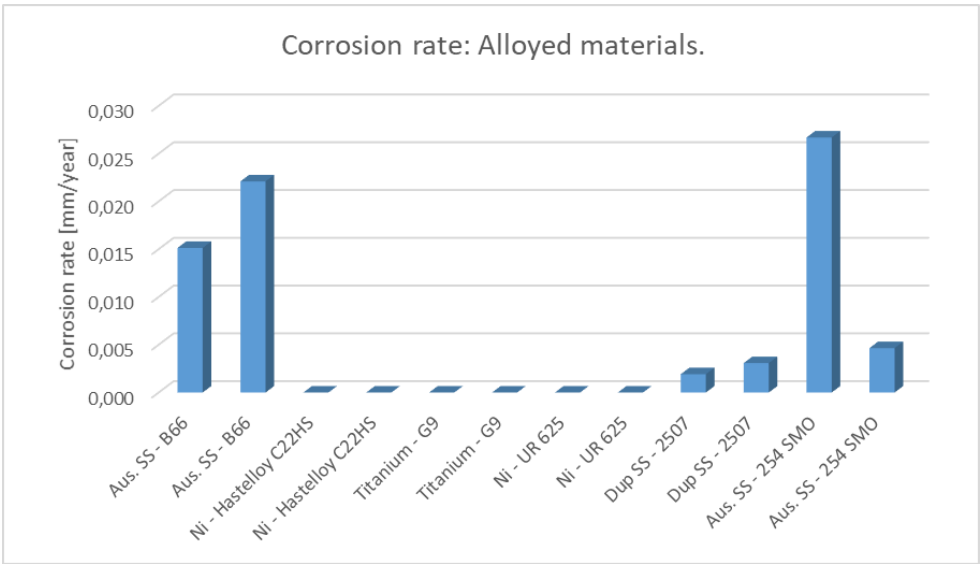

Figure 19. *Corrosion rate for coupons tested for weight loss. Only CRA materials shown.*

Mean value for all materials were calculated as shown in Table 6

Table 6. *Corrosion rate for materials tested as a mean value of two coupons.*

Material	Corr. Rate [mm/year]
CS - API K55	2,310
Aus. SS – S31266 (B66)	0,019
Ni – NO6022 (C22HS)	0,000
Titanium – R56320 (G9)	0,000
Ni – NO6625 (UR 625)	0,000
Dup SS – S32507 (2507)	0,002
Aus. SS – S31254 (254 SMO)	0,016

In Figure 20 the mean value of two weight loss coupons is shown. In Figure 21 the CRA materials are shown. As noted the value for S31254 is higher than predicted as discussed earlier.

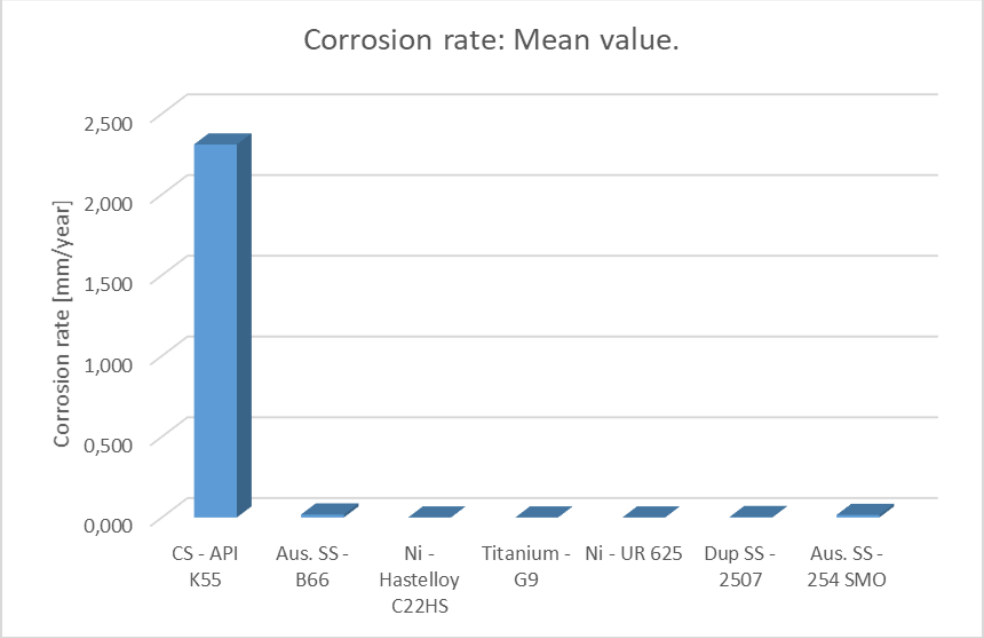

Figure 20. *Corrosion rate as a mean value from two coupons. All materials.*

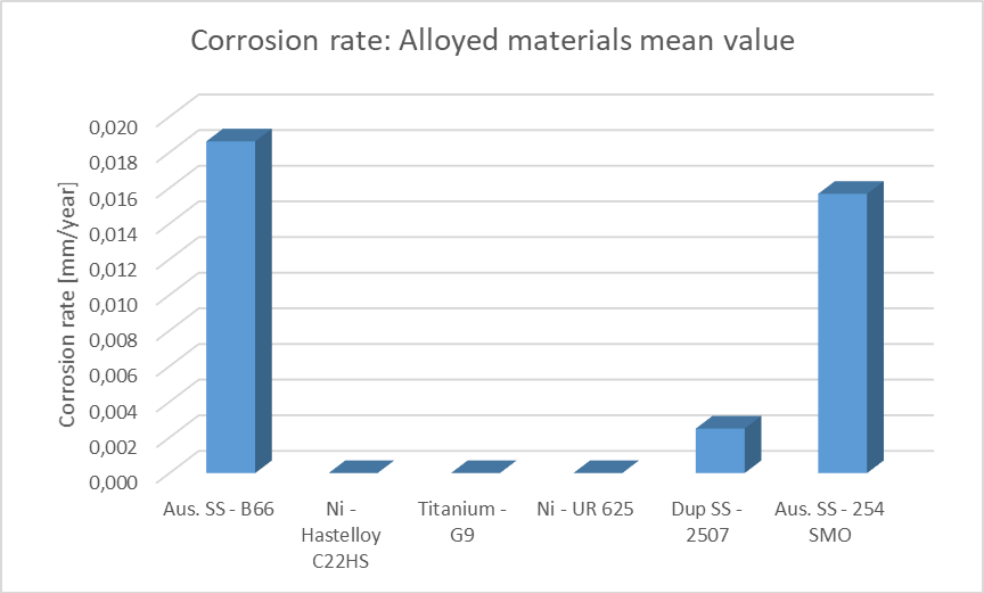

Figure 21. *Corrosion rate for CRA material tested as a mean value from two weight loss coupons for each material.*

For comparison, with earlier weight loss measurements within the EU funded H2020 project GeoWell of the same materials obtained from the same plate or pipes at 450°C superheated steam, test results are shown in Figure 22. It should be noted that coupons sizes were not identical. Same scale (see Figure 15) was used for all samples from both fields.

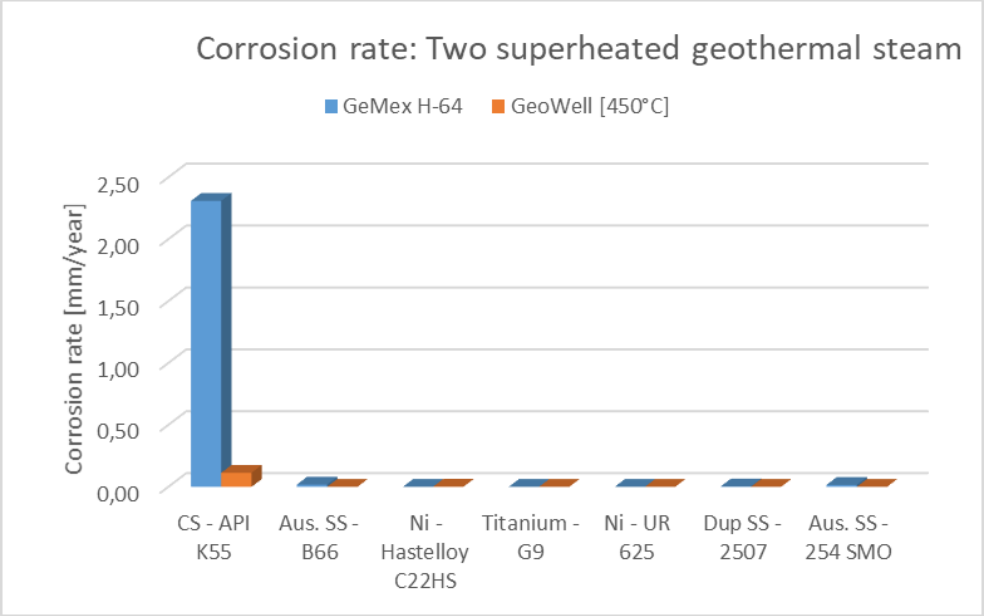

Figure 22. *Corrosion rate measured from weight loss measurements in Los Humeros well H-64 and the Reykjanes Geothermal site in Iceland well RN-35.*

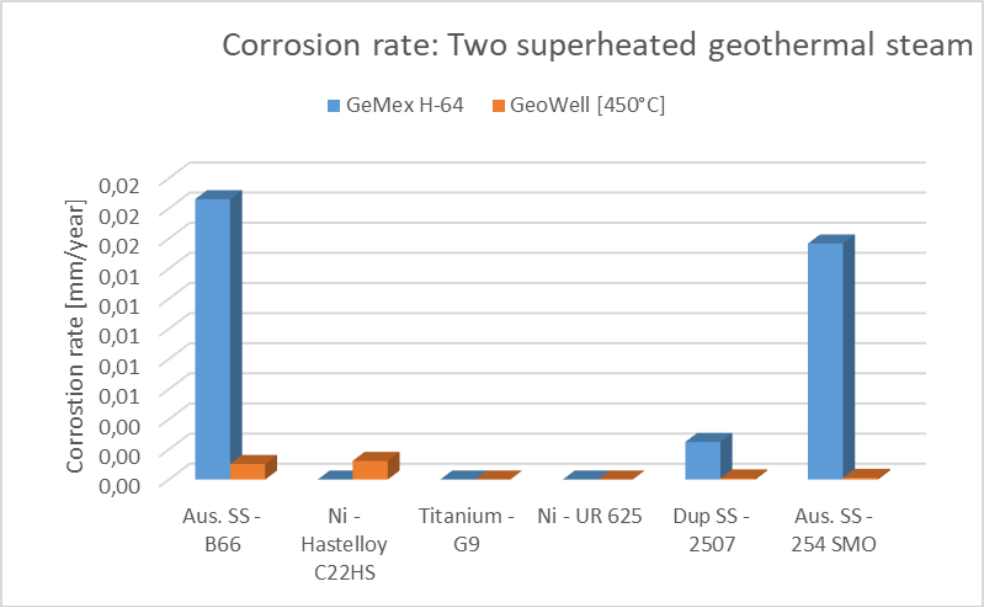

Figure 23. *Corrosion rate for CRA tested in Los Humeros well H-64 and the Reykjanes Geothermal site in Iceland well RN-35.*

7.3 Slow strain tensile testing

For tensile testing, a Satec Model 8801 tensile testing machine with an Instron model 2620-601 extensometer was used. Testing were performed at the company Metalinspec, Laboratorio de Pruebeas according to ASTM E8 with internal procedure COP-ML-40. Tensile specimens were machined from samples tested downhole in Los Humeros for two weeks, see Figure 5 specimens before testing and Figure 9, specimens received from testing. In total three tensile specimens were received from each material where of two were machined according to ISO/DIS 11960 and EN 10 002 part 2 for each location, see Figure 24. One sample of each material was transported to Iceland and is kept as a reserve.

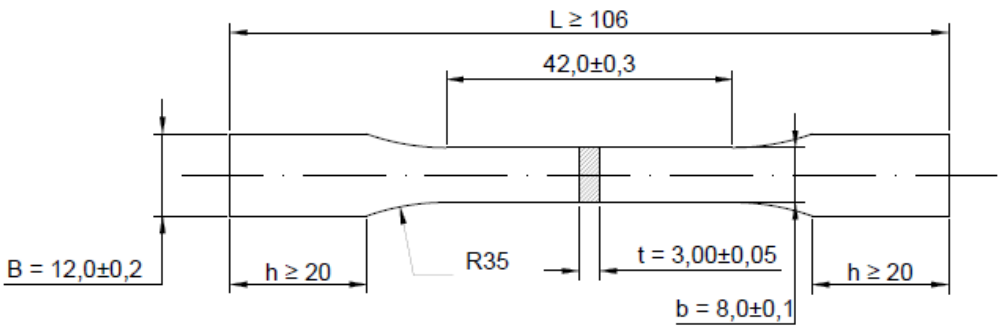

Figure 24. *Drawing of tensile test specimens. Testing speed was set as slow strain testing at 0.15mm/min.*

Results from tensile testing are shown in Table 7. Comparison is given with values from material Manufacurer or material standards. All values are from testing at ambient temperature of around 20°C. Values failing to reach material standard are marked in red, some values are not marked as they are very close to minimum value.

In Figure 25 to Figure 31 graps are shown from the tensile testing.

Table 7. *Slow strain tensile testing of two specimen's pr. material. Values from manufacturer or material standards are shown for comparison. Red marked text indicate that testing reveal that value lies below given minimum by standard or manufacturer.*

No.	Type	Name	$Sy_{0,2}$ [MPa]		Su [MPa]		A_5 [%]	
			Test	Manufacturer Or Standard	Test	Manufacturer Or Standard	Test	Manufacturer Or Standard
SA01 SA01	Carbon steel	API K55	439,7 441,1	379-551	710,9 712,5	>655	24,26 17,68	>19
SA05 SA05	Austenitic SS	S31266 (B66)	429,7 452,7	>420	798,7 813,8	>750	48,96 49,56	>50
SA06 SA06	Nickel alloy	N06022 (C-22HS)	1190,4 1225,4	1286,5	1300,9 1310,7	1314,8	9,18 10,32	17,2
SA08 SA08	Titanium	R56320 (Grade 9)	652,9 641,3	666 824	810,7 784,1	793 824	10,86 12,88	15 16
SA10 SA10	Nickel based alloy	NO6625 (UR625)	525,9 485,1	>490*	905,3 917,1	>905*	39,70 42,80	>49
SA14 SA14	Super Duplex SS	S32507 (UR2507)	651,9 644,2	>540	851,8 849,4	>780	26,4 31,76	>25
SA17 SA17	Austenitic SS	S31254 (254 SMO)	440,6 383,2	>310	729,9 708,1	655-850	42,82 46,78	>35

* Cold rolled and mill-annealed sheet (1050°C)

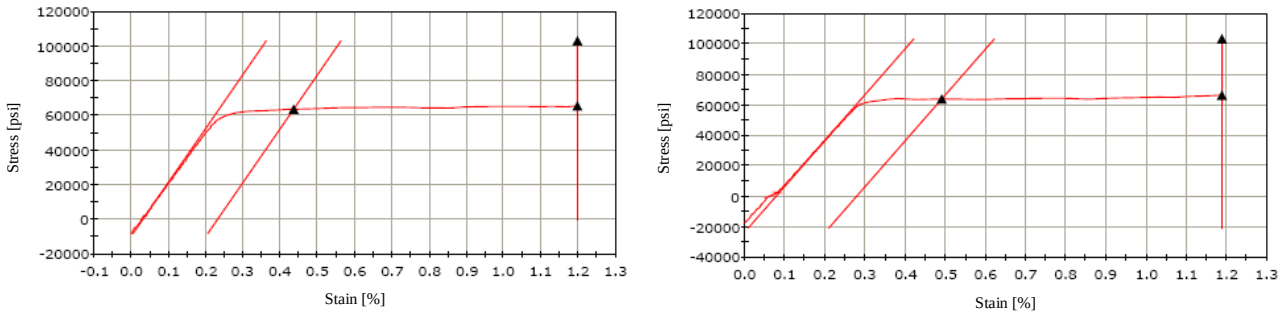

Figure 25. *Tensile testing curves for Carbon steel API K55.*

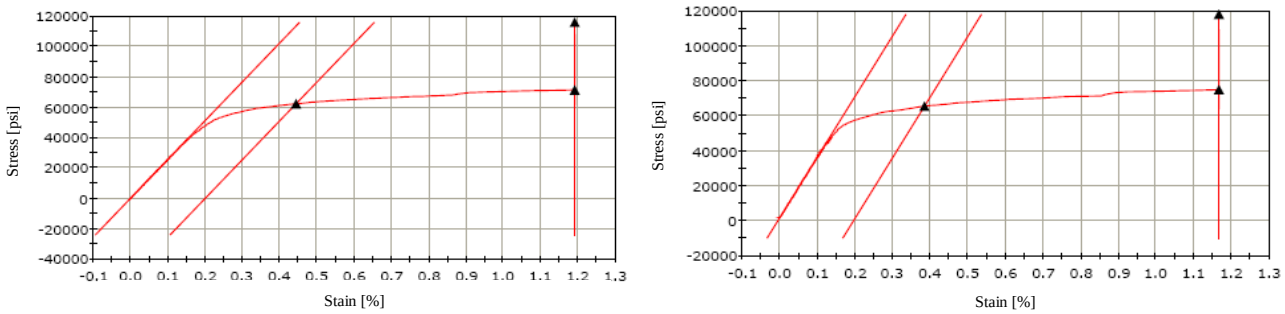

Figure 26. *Tensile testing curves for Super Austenitic stainless steel S31266 (B66).*

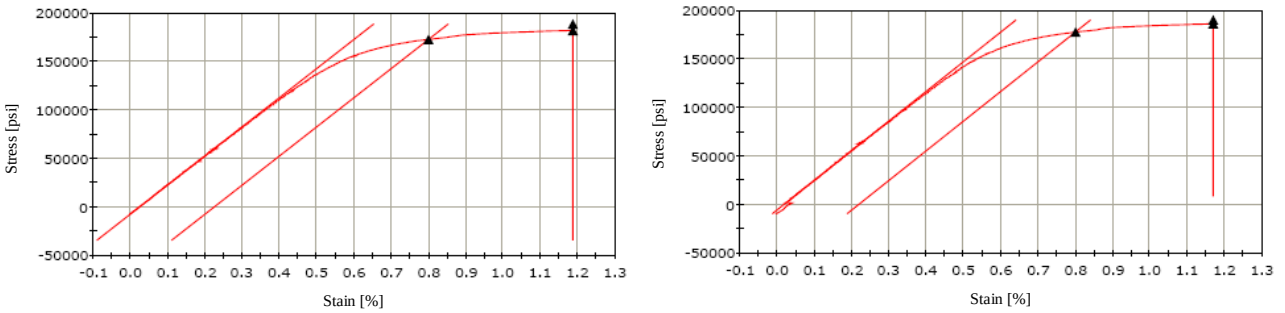

Figure 27. *Tensile testing curves for Nickel alloy NO6022.*

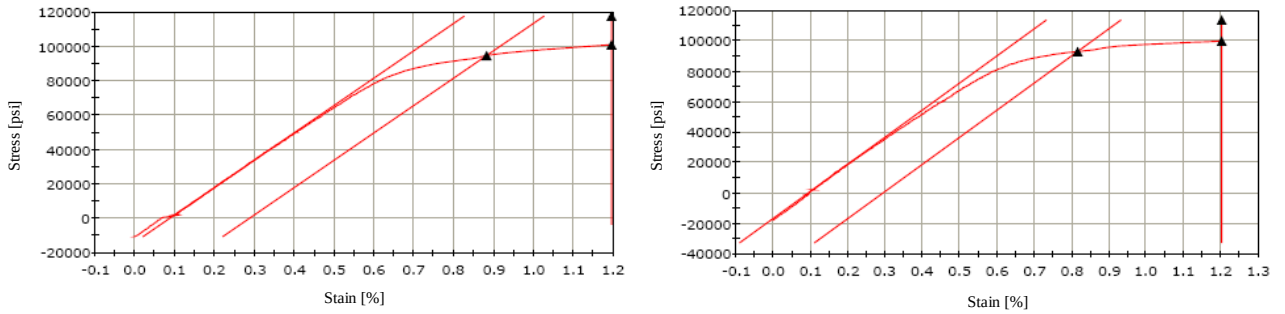

Figure 28. *Tensile testing curves for Titanium R56320 - grade 9.*

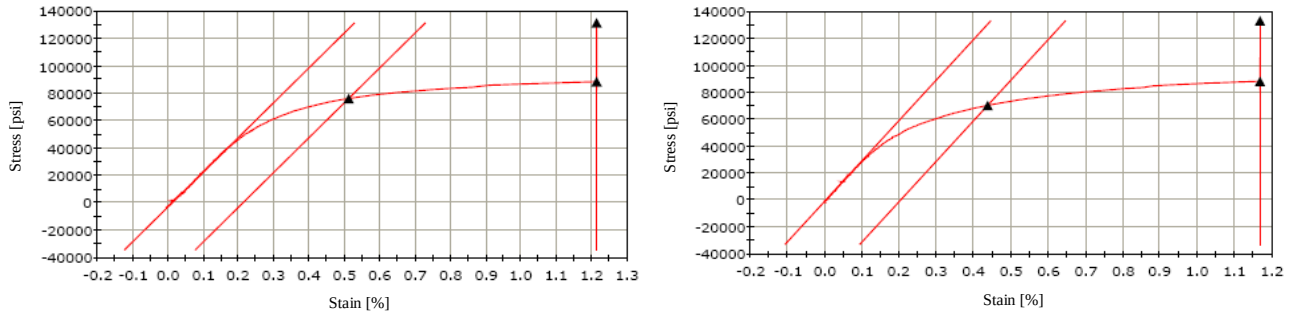

Figure 29. *Tensile testing curves for Nickel alloy NO6625.*

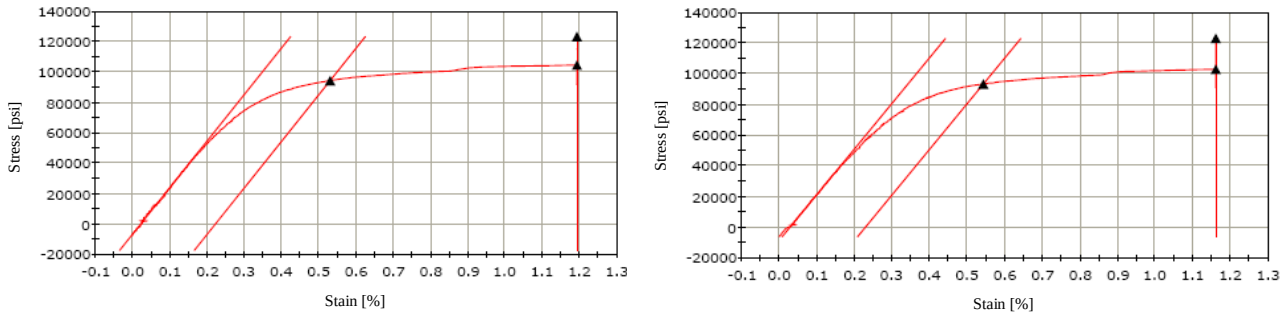

Figure 30. *Tensile testing curves for Super Duplex stainless steel S32507.*

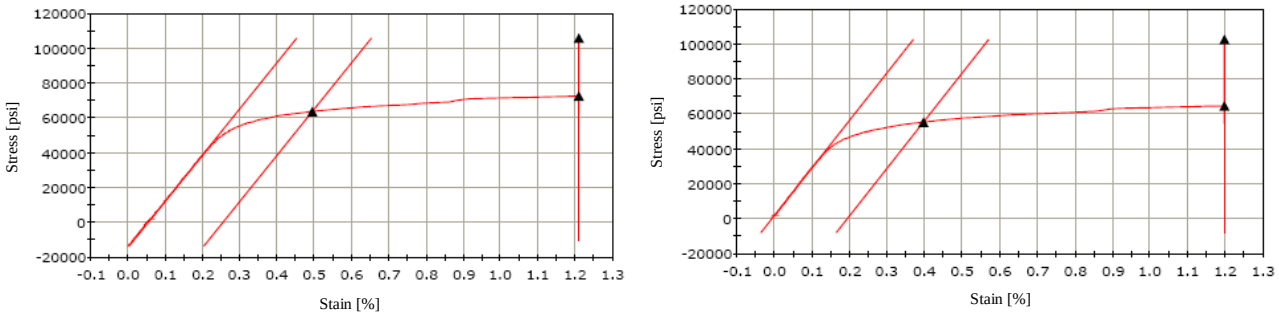

Figure 31. *Tensile testing curves for Super Austenitic stainless steel S31254 (254SMO)*

8 Conclusion

In total 7 alloys were tested for corrosion in Los Humeros well H-64, downhole at 1290m for a period of two weeks. The alloys ranked from medium carbon steel commonly used for casings to high alloyed Nickel and Titanium grades. The main findings are that the corrosion rate for medium carbon steel is very high, normally accepted corrosion rate in geothermal operations is 0.1 mm/year but in well H-64 the medium carbon steel grade K55 was measured with 2.31 mm/year as an average from two cupons tested. All other alloys had lower corrosion rate, below 0.1 mm/year. For the Corrosion Resistant Alloys (CRA) the Super Austenitic Stainless steel B66 showed highest corrosion rate of 0.019 mm/year which was not expected as the lower alloyed type S31217 (254SMO) was with 0.016 mm/year although one of two specimens tested for S3127 revealed higher value than expected. S31217 normally has the same corrosion rate as the Super Duplex grade S32507 and the lower value for S31217 did match that expectations. For other CRA the Nickel and Titanium alloys showed no sign of corrosion. No erosion marks were found by visual inspection of the samples. Although not detected, erosion could be a significant problem in H64 due to very high content of Total Dissolved Solids (TDS) as can be seen in Table 1.

XRD diffraction patterns were taken of corrosion products from the medium carbon steel and the two Super Austenitic grades. These steels were found to have the highest weight loss. The patterns revealed that Iron had dissolved probably from the samples and formed Iron compounds (pyrrhotite).

Tensile testing revealed that some of the CRA materials have lost some strength and ductility compared to standard or manufacturer limits. This is the case with the Nickel alloys and Titanium grade 9.

Material testing revealed in this deliverable has shown that materials subjected to the conditions downhole in well H-64 are suffering from the corrosive environment. Medium carbon steel is

suffering from very high corrosion rate and is not a proper choice for the production casing and liner. Nickel alloys and Titanium show no sign of surface corrosion but the result from tensile testing indicate that to some extend the structural damages most likely from Hydrogen is reducing strength or ductility of the materials. Super Duplex Stainless Steel is performing well but has the limitation that it cannot be used at temperatures higher than 250°C. Super Austenitic Stainless Steels perform well in this study, both with regards to corrosion rate and in tensile tests.

9 References

Karlsdottir S.N. and Thorbjornsson I.O. (2013). *Corrosion testing down-hole in sour high temperature geothermal well in Iceland. NACE,* January 2013. International Corrosion Conference Series.

Karlsdottir, S.N., Ragnarsdottir, K.R., Thorbjornsson, I.O. and Einarsson A. (2015). Corrosion testing in superheated geothermal steam in Iceland. *Geothermics 53* (2015) 281-290.

Tello, E., Mahendra P. Verma, Rigoberto Tovar A. (2000) Origin of acidity in the Los Humeros, Mexico, Geothermal reservoir. *Proceedings World Geothermal Congress 2000. Kyushu-Tohoku, Japan 2000.*

Thorbjornsson, I. (1995). Corrosion fatigue testing of eight different steels in an Icelandic geothermal environment. *Materials and Design, volume 16*.

Thorbjornsson, I.O., Karlsdottir, S.N., Einarsson, A. and Ragnarsdottir, K.R. (2015). Materials for Geothermal Steam Utilization at Higher Temperatures and Pressure. *World Geothermal Congress 2015, Melbourne, Australia.*